


Intrinsic Low-Temperature Magnetism in SmB_6 S. Gheidi,¹ K. Akintola,¹ K. S. Akella,¹ A. M. Côté,^{1,2} S. R. Dunsiger,^{1,3} C. Broholm,^{4,5,6}
W. T. Fuhrman,⁷ S. R. Saha,⁷ J. Paglione,^{7,6} and J. E. Sonier^{1,6}¹*Department of Physics, Simon Fraser University, Burnaby, British Columbia V5A 1S6, Canada*²*Kwantlen Polytechnic University, Richmond, British Columbia V6X 3X7, Canada*³*Centre for Molecular and Materials Science, TRIUMF, Vancouver, British Columbia V6T 2A3, Canada*⁴*Institute for Quantum Matter and Department of Physics and Astronomy, The Johns Hopkins University, Baltimore, Maryland 21218, USA*⁵*Department of Materials Science and Engineering, The Johns Hopkins University, Baltimore, Maryland 21218, USA*⁶*Canadian Institute for Advanced Research, Toronto, Ontario M5G 1Z8, Canada*⁷*Center for Nanophysics and Advanced Materials, Department of Physics, University of Maryland, College Park, Maryland 20742, USA* (Received 21 May 2019; revised manuscript received 29 July 2019; published 7 November 2019)

By means of new muon spin relaxation experiments, we disentangle extrinsic and intrinsic sources of low-temperature bulk magnetism in the candidate topological Kondo insulator (TKI) SmB_6 . Results on Al-flux-grown SmB_6 single crystals are compared to those on a large floating-zone-grown ^{154}Sm $^{11}\text{B}_6$ single crystal in which a 14 meV bulk spin exciton has been detected by inelastic neutron scattering. Below ~ 10 K, we detect the gradual development of quasistatic magnetism due to rare-earth impurities and Sm vacancies. Our measurements also reveal two additional forms of intrinsic magnetism: (1) underlying low-energy (~ 100 meV) weak magnetic moment ($\sim 10^{-2} \mu_B$) fluctuations similar to those detected in the related candidate TKI YbB_{12} that persist down to millikelvin temperatures, and (2) magnetic fluctuations consistent with a 2.6 meV bulk magnetic excitation at zero magnetic field that appears to hinder surface conductivity above ~ 4.5 K. We discuss potential origins of the magnetism.

DOI: [10.1103/PhysRevLett.123.197203](https://doi.org/10.1103/PhysRevLett.123.197203)

In recent years, there has been a concerted effort to determine whether the intermediate-valence compound SmB_6 is a strongly correlated three-dimensional (3D) topological insulator (TI). A 3D TI possesses an insulating bulk and topologically protected metallic surface states, where the electron spin is locked perpendicular to the crystal momentum by strong spin-orbit coupling [1,2]. What makes SmB_6 so different from known 3D TIs [3–5] is that it hosts an unconventional insulating bulk gap that forms due to Kondo hybridization of itinerant Sm $5d$ electrons with localized Sm $4f$ states. As expected for a 3D TI, experiments on SmB_6 have established the facts that metallic surface states dominate the electrical transport below $T \sim 5$ K [6–8] and that a truly insulating bulk exists down to at least 2 K [9]. Yet there is ongoing debate as to whether the surface states are of topological origin. While scanning tunneling microscopy experiments support the existence of heavy in-gap topological Dirac fermion states at the predicted locations in the surface Brillouin zone [10], Dirac points have yet to be clearly observed by angle resolved photoemission spectroscopy (ARPES) [11]. Furthermore, spin-polarized ARPES experiments aimed at determining whether the surface states have the topological property of spin-momentum locking have reached very different conclusions [12,13].

While a true Kondo insulator is nonmagnetic, low-temperature magnetism is clearly present in SmB_6 . There is a field-dependent divergence of the temperature dependence of the bulk magnetic susceptibility $\chi(T)$ below ~ 15 K, originally attributed to bare Sm^{3+} ($4f^5$) magnetic moments, but later ascribed to paramagnetic rare-earth impurities incorporated during sample growth [14,15]. Magnetic impurities, which can destroy the topological protection of surface states by breaking time-reversal symmetry, are also responsible for a large field-induced enhancement of the thermal conductivity [16].

There is also evidence for intrinsic bulk magnetic excitations in SmB_6 . A 14 meV bulk spin exciton has been detected by inelastic neutron scattering (INS) [17–19], and there are reports of lower-energy bulk magnetic excitations potentially relevant to the temperature range over which SmB_6 exhibits topological behavior. Nuclear magnetic resonance (NMR) measurements indicate the existence of intrinsic bulk magnetic in-gap states separated from the conduction band by a 2.6 meV gap that shrinks with increasing field [20] and muon spin relaxation (μSR) experiments detect slowly fluctuating internal magnetic fields that persist down to at least 0.02 K [21–23]. Recently, muon Knight shift measurements on SmB_6 at $H = 60$ kOe have provided evidence for bulk magnetic excitations

governed by an ~ 1 meV thermal activation energy [24]. While an additional $\lesssim 1$ meV spin exciton is predicted [25], the magnetic excitations at $H = 60$ kOe may derive from the zero-field-extrapolated 2.6 meV magnetic in-gap states detected by NMR. A $\lesssim 2.6$ meV spin exciton may hinder topological behavior via spin-flip scattering of the metallic surface states [26,27]. Surprisingly, however, no collective magnetic excitation has been detected by INS below 14 meV [28].

Here we report on new zero-field (ZF) and longitudinal-field (LF) μ SR measurements of SmB_6 that enable us to disentangle extrinsic and intrinsic sources of low-temperature magnetism. Our measurements were performed on a mosaic of hundreds of randomly oriented small aluminum- (Al-) flux-grown SmB_6 single crystals, and on a large doubly isotope enriched $^{154}\text{Sm}^{11}\text{B}_6$ single crystal grown by the floating zone (FZ) method. The latter is the same $^{154}\text{Sm}^{11}\text{B}_6$ single crystal in which a 14 meV spin exciton has been detected by INS [17–19].

Flux-grown SmB_6 single crystals are known to contain Al inclusions [29]. Pure Al does not contain electronic moments, and while muons landing in the Al inclusions may sense static nuclear dipole fields, these are decoupled on the same field scale as the B nuclear moments in our LF experiments. Samarium (Sm) vacancies, which act as “Kondo holes” in the strongly correlated state of SmB_6 , are more prevalent in FZ-grown single crystals [29]. Theoretically, a finite concentration of Sm vacancies introduces an impurity band in the hybridization gap and gives rise to a Curie-Weiss-like susceptibility [30]. They also adversely affect spin excitons, as evidenced by a Sm-vacancy-induced suppression of the 16–18 meV exciton feature observed by Raman spectroscopy [31].

Figure 1 shows representative $\chi(T)$ data for the two samples studied here and for one of the Al-flux-grown single crystals investigated in Ref. [24]. No magnetic hysteresis was found in any of the samples. The magnetic susceptibility over much of the temperature range is a sum of contributions from the $4f^6 \text{Sm}^{2+}$ and $4f^5 5d^1 \text{Sm}^{3+}$ ion configurations [32]. There is a pronounced low- T upturn in $\chi(T)$ for the current samples, and the overall susceptibility is greater in the larger $^{154}\text{Sm}^{11}\text{B}_6$ single crystal. Both features are clearly of extrinsic origin.

Figure 2 shows typical ZF- and weak LF- μ SR asymmetry spectra for the $^{154}\text{Sm}^{11}\text{B}_6$ single crystal which are reasonably described by

$$A(t) = a_0 G_{\text{KT}}(\Delta, t, H_{\text{LF}}) e^{-[\lambda(T)t]^\beta}, \quad (1)$$

where $G_{\text{KT}}(\Delta, t, H_{\text{LF}})$ is the static Gaussian Kubo-Toyabe function [33] intended to account for the temperature-independent relaxation caused by the nuclear moments. It assumes a Gaussian field distribution of width Δ/γ_μ (where $\gamma_\mu/2\pi$ is the muon gyromagnetic ratio) and is dependent on the applied longitudinal field H_{LF} . The LF- μ SR spectra in

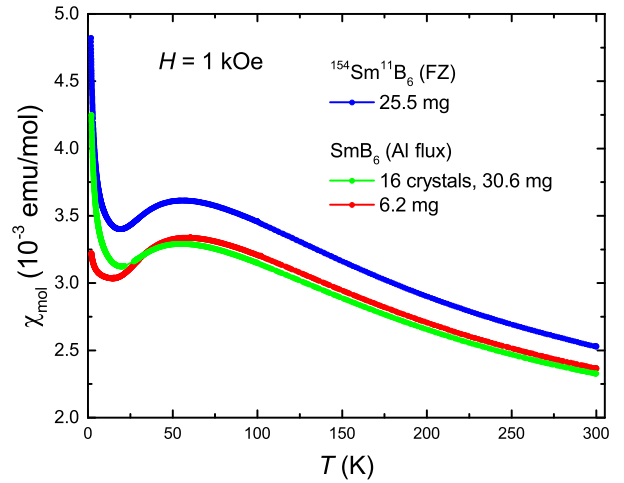


FIG. 1. Temperature dependence of the bulk magnetic susceptibility at $H = 1$ kOe for a piece of the FZ-grown $^{154}\text{Sm}^{11}\text{B}_6$ single crystal, a mosaic of 16 of the Al-flux-grown SmB_6 single crystals, and one of the Al-flux-grown single crystals studied in Ref. [24].

Fig. 1(b) were recorded for $H_{\text{LF}} = 100$ Oe, which is sufficient to completely decouple the muon spin from the nuclear dipole fields. The stretched-exponential function in Eq. (1) accounts for additional sources of magnetic

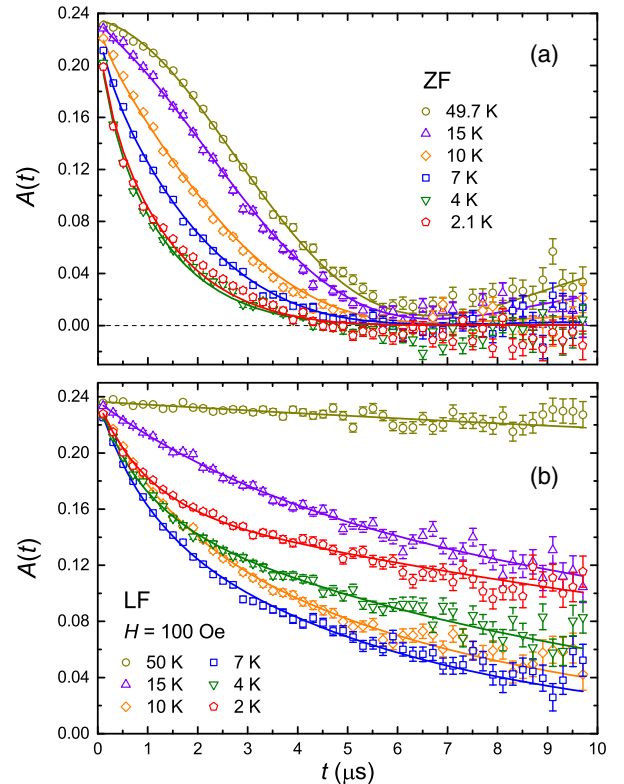


FIG. 2. Representative (a) ZF- and (b) LF- μ SR asymmetry spectra recorded on the $^{154}\text{Sm}^{11}\text{B}_6$ single crystal. The LF- μ SR spectra were recorded for a field $H_{\text{LF}} = 100$ Oe applied parallel to the initial muon spin polarization. The solid curves through the data points are fits to Eq. (1).

field in the sample. Global fits of the ZF and 100 Oe LF spectra assuming β is independent of temperature, yield $\beta = 0.562(5)$ and $0.552(9)$ for the Al-flux-grown sample, and $\beta = 0.699(2)$ and $0.658(3)$ for the FZ-grown single crystal. The ZF fits also yield $\Delta = 0.2336(6) \mu\text{s}^{-1}$ and $\Delta = 0.2589(7) \mu\text{s}^{-1}$ for the Al-flux and FZ-grown samples, respectively. The ZF values of Δ and β are somewhat different from those obtained in previous μSR studies of SmB_6 [21–23], highlighting variations in sample quality.

The temperature dependence of the fitted values of λ for the two samples is shown in Fig. 3. Below ~ 20 K, the ZF value of λ increases more rapidly in the $^{154}\text{Sm}^{11}\text{B}_6$ single crystal. This behavior is qualitatively similar to previous findings [21], although the difference between the FZ- and Al-flux-grown single crystals here is more extreme. In the earlier ZF- μSR studies, a broad peak in $\lambda(T)$ was observed near 4 to 5 K [21–23]. The sharpness of this feature, however, is sample dependent. Here both samples display a maximum in $\lambda(T)$ for ZF near 4.5 K. Below ~ 10 K, the 100 Oe LF and ZF values of $\lambda(T)$ diverge in both samples. The significant reduction of λ by the 100 Oe field indicates the gradual development of weak local quasistatic magnetic fields as the temperature is lowered toward 2 K. In what follows, we demonstrate via LF- μSR results up to 4 kOe that this magnetism is dependent on the sample preparation.

Above ~ 20 K, we find the stretched-exponential relaxation function in Eq. (1) may be replaced by a pure exponential. Figure 4(a) shows $\lambda(H_{\text{LF}})$ at 50 K for both samples, obtained from an analysis with $\beta = 1$. Biswas *et al.* [21] previously showed that the relaxation rate $\lambda(H_{\text{LF}})$ below $H_{\text{LF}} \sim 100$ Oe exhibits a broad peak centered near

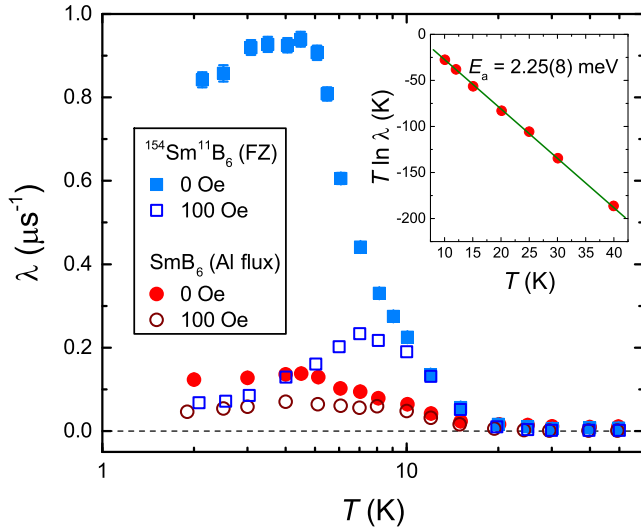


FIG. 3. Temperature dependence of the ZF- μSR (solid symbols) and 100 Oe LF- μSR (open symbols) relaxation rate λ for the FZ-grown $^{154}\text{Sm}^{11}\text{B}_6$ and Al-flux-grown SmB_6 single crystals. (Inset) Temperature dependence of the ZF data for the Al-flux-grown sample at $T \geq 10$ K, shown as an Arrhenius plot in the form $T \ln \lambda$ vs T . The green line is a linear fit with intercept E_a/k_b .

40 Oe due to an avoided level crossing resonance (ALCR)—presumably due to a matching of the Zeeman splittings of the muon and B nuclear spins. While the influence of the ALCR is evident below 100 Oe, at higher field $\lambda(H_{\text{LF}})$ is independent of field and identical in the two samples. Moreover, the average value of $\lambda(H_{\text{LF}})$ between 100 Oe and 4 kOe is in good agreement with the ZF values of λ at 50 K in Fig. 3. Thus it is clear that the muons sense fast fluctuating internal fields of a similar rate in both samples at 50 K.

Figures 4(b) and 4(c) show $\lambda(H_{\text{LF}})$ at 4.5 and 2 K obtained from fits to Eq. (1) with Δ and β fixed to the values determined from the analysis of the ZF- μSR spectra for each sample. In addition, we show results for the $^{154}\text{Sm}^{11}\text{B}_6$ single crystal at 2 K from fits assuming the

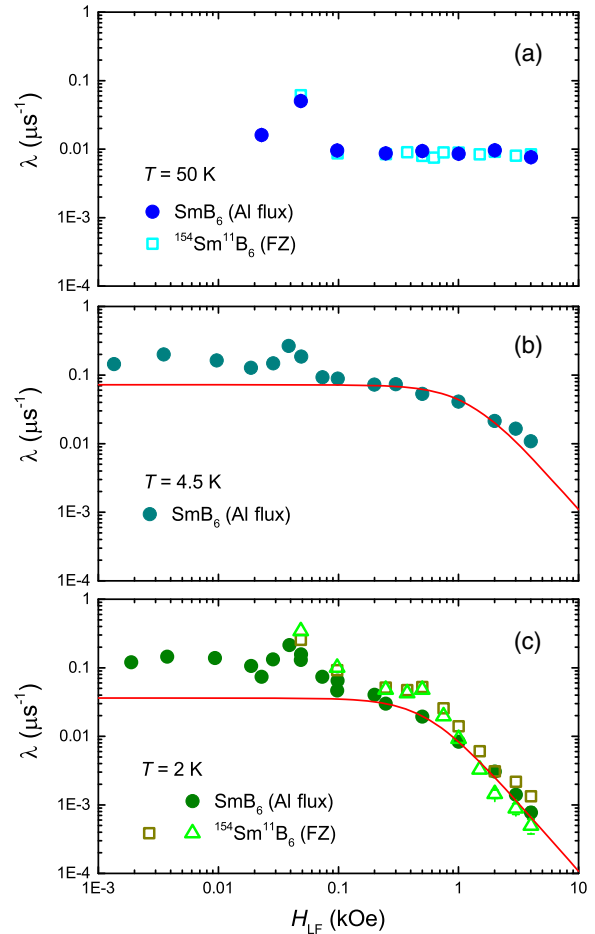


FIG. 4. Field dependence of the relaxation rate λ obtained from fits of the LF- μSR asymmetry spectra at (a) 50, (b) 4.5, and (c) 2 K. Note that λ is a “pure” exponential relaxation rate in (a), but a stretched-exponential relaxation rate in (b) and (c). The solid green circles and open brown squares in (c) are from fits assuming the ZF values $\beta = 0.562$ and $\beta = 0.699$, respectively. The open green triangles are results for the $^{154}\text{Sm}^{11}\text{B}_6$ single crystal from fits assuming the ZF value $\beta = 0.562$ for the Al-flux-grown sample. The solid red curves in (b) and (c) are fits of the $H_{\text{LF}} > 100$ Oe data for the Al-flux-grown single crystals to Eq. (2).

Al-flux-grown value $\beta = 0.562$. Above 100 Oe, there is good agreement between $\lambda(H_{\text{LF}})$ for the two samples, and the data are well described by the Redfield formula [34]

$$\lambda(H_{\text{LF}}) = \frac{\lambda(H_{\text{LF}} = 0)}{1 + (\gamma_{\mu} H_{\text{LF}} \tau)^2}, \quad (2)$$

where $\lambda(H_{\text{LF}} = 0) = 2\gamma_{\mu}^2 \langle B_{\text{loc}}^2 \rangle \tau$, and where $\langle B_{\text{loc}}^2 \rangle$ is the mean of the square of the transverse components of a local magnetic field fluctuating at a rate $1/\tau$. Equation (2) is strictly valid for fast field fluctuations in a Gaussian distribution with a single fluctuation rate $1/\tau$, whereas a stretched-exponential relaxation often signifies a distribution of fluctuation rates. Nevertheless, the Redfield equation is adequate for achieving an approximate quantitative understanding of the data, provided that the applied field does not modify the magnetic fluctuation spectrum. A fit of the $\lambda(H_{\text{LF}} > 100 \text{ Oe})$ data for the Al-flux-grown single crystals to Eq. (2) yields $\lambda(H_{\text{LF}} = 0) = 0.0361(6) \mu\text{s}^{-1}$, $\tau = 2.15(6) \times 10^{-8} \text{ s}$, and $B_{\text{loc}} = 10.8(5) \text{ G}$ at 2 K, and $\lambda(H_{\text{LF}} = 0) = 0.072(4) \mu\text{s}^{-1}$, $\tau = 0.9(1) \times 10^{-8} \text{ s}$, and $B_{\text{loc}} = 23(5) \text{ G}$ at 4.5 K. We note that similar values are obtained from fits where β is free to vary with H_{LF} [35]. The fitted value of $\lambda(H_{\text{LF}} = 0)$ at 2 K is nearly 3.5 times smaller than the ZF value of λ for the Al-flux-grown SmB_6 single crystals, and ~ 23 times smaller than the ZF value of λ for the FZ-grown $^{154}\text{Sm } ^{11}\text{B}_6$ single crystal (see Fig. 3). This implies that a weak LF completely decouples the muon spin from a source of bulk magnetism, distinct from that of the nuclear moments. Since the difference between the fitted value of $\lambda(H_{\text{LF}} = 0)$ and the ZF value of λ is much greater for the $^{154}\text{Sm } ^{11}\text{B}_6$ single crystal, the magnetism is likely due to a greater concentration of Sm vacancies and perhaps rare-earth impurities. Contrarily, the similarity of $\lambda(H_{\text{LF}})$ for the two samples above 100 Oe indicates that there is at least one other source of intrinsic bulk magnetism, which at 2 K gives rise to fluctuating magnetic fields of frequency on the order of 10^7 Hz .

In the absence of a low-energy spin exciton, the existence of the intrinsic magnetism is surprising. The implanted positive muon (μ^+) senses the localized Sm $4f$ moments via the magnetic dipole interaction and through an indirect Ruderman-Kittel-Kasuya-Yosida interaction that spin polarizes the conduction electrons at the muon site. In zero field, the total field at the μ^+ site \mathbf{B}_{μ} is the vector sum of the corresponding dipolar (\mathbf{B}_{dip}) and hyperfine contact (\mathbf{B}_{hf}) fields. The opening of the Kondo gap in SmB_6 is complete by $T \sim 30 \text{ K}$ [11,36]. Consequently, \mathbf{B}_{dip} and \mathbf{B}_{hf} are expected to vanish at $T \ll 30 \text{ K}$ due to complete screening of the Sm $4f$ moments by the conduction electrons and the absence of a screening cloud of conduction electrons about the μ^+ .

If the intrinsic magnetism is associated with populating a low-energy spin exciton state, the ZF relaxation rate should obey an Arrhenius law $\lambda = \lambda_0 \exp(E_a/k_B T) \propto \tau$.

Unfortunately, any such behavior for the $^{154}\text{Sm } ^{11}\text{B}_6$ single crystal is masked by the large Sm vacancy or impurity contribution. The ZF relaxation rate for the Al-flux-grown sample does exhibit an Arrhenius behavior for $T \geq 10 \text{ K}$, characterized by an activation energy $E_a = 2.25(8) \text{ meV}$ (Fig. 3 inset). Combined with the lower value $E_a \sim 1 \text{ meV}$ determined from 60 kOe transverse-field μSR measurements of the relaxation rate in similar Al-flux-grown single crystals [24], these results are compatible with the field-dependent contribution to the ^{11}B NMR spin-lattice relaxation rate—which has been explained by in-gap magnetic states separated from the conduction band by a 2.6 meV gap that shrinks with increasing field and closes by 140 kOe [20]. An $\sim 2.6 \text{ meV}$ zero-field gap has also been observed by magnetotransport measurements [37], and in the low-energy electrodynamic response spectra of SmB_6 in the far-infrared range [38]. A 2.6 meV magnetic exciton is predicted to arise from a competition between the magnetic $4f^5$ and nonmagnetic $4f^6$ multiplets [39]. Based on solutions of the single-site Anderson impurity model, $1.74 \mu_B$ local magnetic moments are generated via excitation of a triplet state situated 2.6 meV in energy above an intermediate-valence nonmagnetic singlet ground state. However, one then expects a sharp neutron energy transfer peak at 2.6 meV or a dispersive peak associated with a collective mode of the localized moment system due to intersite interactions. The $\sim 2.6 \text{ meV}$ magnetic excitation may instead be connected to recent theoretical work that shows donor impurities in SmB_6 produce a midgap impurity band with a corresponding ionization energy of 1 to 5 meV [40].

Below 4.5 K, the LF results clearly show that spin freezing in SmB_6 has an extrinsic origin and there exist weak intrinsic fields ($B_{\text{loc}} \sim 10.8 \text{ G}$) that fluctuate too slowly ($1/\tau \sim 47 \text{ MHz}$) to originate from a magnetic excitation gap on the order of 1 meV. The latter is similar to μSR findings in the Kondo insulator YbB_{12} , which indicate the presence of slowly fluctuating ($1/\tau \sim 60 \text{ MHz}$) weak internal fields ($B_{\text{loc}} = 5.4 \text{ G}$) below $\sim 5 \text{ K}$ [41]. The values of B_{loc} are consistent with very small localized Sm and Yb magnetic moments ($\sim 10^{-2} \mu_B$). Since there is no further change in λ down to millikelvin temperatures [21,23,41], the small magnetic moment may indicate that the carrier density in these compounds is insufficient to completely Kondo screen the localized $4f$ magnetic moments. On the other hand, μSR experiments on CaB_6 and BaB_6 show the emergence of small random magnetic moments ($\sim 10^{-2} \mu_B/B$) below $\sim 130 \text{ K}$ [42], perhaps associated with intrinsic defects detected in transport measurements of alkaline-earth-metal hexaborides [43]. Here the similarity of the data for the FZ- and Al-flux-grown samples in Fig. 4(c) seems to rule out Sm vacancies, but the weakly dynamic small-moment magnetism may originate from other kinds of intrinsic defects.

In summary, we have shown that there are multiple sources of low- T magnetism in SmB_6 . In addition to underlying persistent slowly fluctuating weak moments,

our experiments provide additional support for a bulk ~ 2.6 meV magnetic excitation. The results on the neutron $^{154}\text{Sm } ^{11}\text{B}_6$ sample demonstrate that enhanced Sm vacancies do not explain why a magnetic excitation of this energy is not observed by INS. Since optical conductivity experiments link the ~ 2.6 meV excitation to charge carrier localization [38], the origin might be connected to intrinsic defects and the creation of very small magnetic moments—such that the neutron cross section is below the noise floor even in the large $^{154}\text{Sm } ^{11}\text{B}_6$ sample. A very weak broad “hump” seen in the specific heat of a FZ-grown, isotopically enriched SmB_6 sample between 4 and 10 K [44] may be a manifestation of this magnetic excitation, as this feature is also observed in the specific heat of our samples. However, in contrast to the strong magnetic field dependence of the ^{11}B NMR $1/T_1$ maximum and μSR relaxation rate in this temperature range, the field dependence of this very small specific heat hump is almost negligible up to 140 kOe. Lastly, we note that there is a similar 2.7 meV electronic excitation [45] and an analogous field-dependent ^{11}B NMR $1/T_1$ maximum [46] in YbB_{12} , suggesting that the sources of the intrinsic low- T magnetism in these two candidate topological Kondo insulators are the same.

We thank P. S. Riseborough and A. B. Shick for the informative discussions. J. P. acknowledges support from the Gordon and Betty Moore Foundation’s EPiQS Initiative through Grant No. GBMF4419, and National Institute of Standards and Technology Cooperative Agreement No. 70NANB17H301. W. T. F. is grateful to the ARCS Foundation and the Schmidt Science Fellows program, in partnership with the Rhodes Trust, for the partial support of this work. J. E. S. acknowledges support from the Natural Sciences and Engineering Research Council of Canada. We thank P. A. Alekseev and J.-M. Mignot for providing access to the $^{154}\text{Sm } ^{11}\text{B}_6$ single crystal.

[1] M. Z. Hasan and C. L. Kane, *Rev. Mod. Phys.* **82**, 3045 (2010).
 [2] X.-L. Qi and S.-C. Zhang, *Rev. Mod. Phys.* **83**, 1057 (2011).
 [3] D. Hsieh, D. Qian, L. Wray, Y. Xia, Y. Hor, R. Cava, and M. Hasan, *Nature (London)* **452**, 970 (2008).
 [4] Y. Xia, D. Qian, D. Hsieh, L. Wray, A. Pal, H. Lin, A. Bansil, D. Grauer, Y. Hor, R. Cava *et al.*, *Nat. Phys.* **5**, 398 (2009).
 [5] Y. Chen, J. Analytis, J.-H. Chu, Z. Liu, S.-K. Mo, X.-L. Qi, H. Zhang, D. Lu, X. Dai, Z. Fang *et al.*, *Science* **325**, 178 (2009).
 [6] D. J. Kim, S. Thomas, T. Grant, J. Botimer, Z. Fisk, and J. Xia, *Sci. Rep.* **3**, 3150 (2013).
 [7] S. Wolgast, C. Kurdak, K. Sun, J. W. Allen, D. J. Kim, and Z. Fisk, *Phys. Rev. B* **88**, 180405(R) (2013).
 [8] P. Syers, D. Kim, M. S. Fuhrer, and J. Paglione, *Phys. Rev. Lett.* **114**, 096601 (2015).

[9] Y. S. Eo, A. Rakoski, J. Lucien, D. Mihalirov, C. Kurdak, P. F. S. Rosa, and Z. Fisk, *Proc. Natl. Acad. Sci. U.S.A.* **116**, 12638 (2019).
 [10] H. Pirie, Y. Liu, A. Soumyanarayanan, P. Chen, Y. He, M. M. Yee, P. F. S. Rosa, J. D. Thompson, D.-J. Kim, Z. Fisk, X. Wang, J. Paglione, D. K. Morr, M. H. Hamidian, and J. E. Hoffman, [arXiv:1810.13419](https://arxiv.org/abs/1810.13419).
 [11] N. Xu, C. E. Matt, E. Pomjakushina, X. Shi, R. S. Dhaka, N. C. Plumb, M. Radović, P. K. Biswas, D. Evtushinsky, V. Zabolotnyy *et al.*, *Phys. Rev. B* **90**, 085148 (2014).
 [12] N. Xu, P. K. Biswas, J. H. Dil, R. S. Dhaka, G. Landolt, S. Muff, C. E. Matt, X. Shi, N. C. Plumb, M. Radović *et al.*, *Nat. Commun.* **5**, 4566 (2014).
 [13] P. Hlawenka, K. Siemensmeyer, E. Weschke, A. Varykhalov, J. Sánchez-Barriga, N. Y. Shitsevalova, A. V. Dukhnenko, V. B. Filipov, S. Gabáni, K. Flachbart *et al.*, *Nat. Commun.* **9**, 517 (2018).
 [14] J. Roman, V. Pavlík, K. Flachbart, T. Herrmannsdörfer, S. Rehm, E. S. Konovalova, and Y. B. Paderno, *Physica (Amsterdam)* **230B–232B**, 715 (1997).
 [15] S. Gabáni, K. Flachbart, V. Pavlík, T. Herrmannsdörfer, E. Konovalova, Y. Paderno, J. Briančin, and J. Trpčevská, *Czech. J. Phys.* **52**, A225 (2002).
 [16] M. E. Boulanger, F. Laliberté, M. Dion, S. Badoux, N. Doiron-Leyraud, W. A. Phelan, S. M. Koohpayeh, W. T. Fuhrman, J. R. Chamorro, T. M. McQueen *et al.*, *Phys. Rev. B* **97**, 245141 (2018).
 [17] P. A. Alekseev, J.-M. Mignot, J. Rossat-Mignod, V. N. Lazukov, and I. P. Sadikov, *Physica (Amsterdam)* **186B–188B**, 384 (1993).
 [18] P. A. Alekseev, J.-M. Mignot, J. Rossat-Mignod, V. N. Lazukov, I. P. Sadikov, E. S. Konovalova, and Y. B. Paderno, *J. Phys. Condens. Matter* **7**, 289 (1995).
 [19] W. T. Fuhrman, J. Leiner, P. Nikolić, G. E. Granroth, M. B. Stone, M. D. Lumsden, L. DeBeer-Schmitt, P. A. Alekseev, J.-M. Mignot, S. M. Koohpayeh *et al.*, *Phys. Rev. Lett.* **114**, 036401 (2015).
 [20] T. Caldwell, A. P. Reyes, W. G. Moulton, P. L. Kuhns, M. J. R. Hoch, P. Schlottmann, and Z. Fisk, *Phys. Rev. B* **75**, 075106 (2007).
 [21] P. K. Biswas, Z. Salman, T. Neupert, E. Morenzoni, E. Pomjakushina, F. von Rohr, K. Conder, G. Balakrishnan, M. C. Hatnean, M. R. Lees *et al.*, *Phys. Rev. B* **89**, 161107(R) (2014).
 [22] P. K. Biswas, M. Legner, G. Balakrishnan, M. C. Hatnean, M. R. Lees, D. McK. Paul, E. Pomjakushina, T. Prokscha, A. Suter, T. Neupert, and Z. Salman, *Phys. Rev. B* **95**, 020410(R) (2017).
 [23] K. Akintola, A. Pal, M. Potma, S. R. Saha, X. F. Wang, J. Paglione, and J. E. Sonier, *Phys. Rev. B* **95**, 245107 (2017).
 [24] K. Akintola, A. Pal, S. R. Dunsiger, A. C. Y. Fang, M. Potma, S. R. Saha, X. Wang, J. Paglione, and J. E. Sonier, *npj Quantum Mater.* **3**, 36 (2018).
 [25] J. Knolle and N. R. Cooper, *Phys. Rev. Lett.* **118**, 096604 (2017).
 [26] G. A. Kapilevich, P. S. Riseborough, A. X. Gray, M. Gulacsi, T. Durakiewicz, and J. L. Smith, *Phys. Rev. B* **92**, 085133 (2015).
 [27] A. Arab, A. X. Gray, S. Nemšák, D. V. Evtushinsky, C. M. Schneider, D.-J. Kim, Z. Fisk, P. F. S. Rosa, T. Durakiewicz,

- and P. S. Riseborough, *Phys. Rev. B* **94**, 235125 (2016).
- [28] W. T. Fuhrman, J. R. Chamorro, P. A. Alekseev, J.-M. Mignot, T. Keller, J. A. Rodriguez-Rivera, Y. Qiu, P. Nikolić, T. M. McQueen, and C. L. Broholm, *Nat. Commun.* **9**, 1539 (2018).
- [29] W. A. Phelan, S. M. Koohpayeh, P. Cottingham, J. A. Tutmaher, J. C. Leiner, M. D. Lumsden, C. M. Lavelle, X. P. Wang, C. Hoffmann, M. A. Siegler *et al.*, *Sci. Rep.* **6**, 20860 (2016).
- [30] P. Schlottmann, *Phys. Rev. B* **46**, 998 (1992).
- [31] M. E. Valentine, S. Koohpayeh, W. A. Phelan, T. M. McQueen, P. F. S. Rosa, Z. Fisk, and N. Drichko, *Phys. Rev. B* **94**, 075102 (2016).
- [32] J. C. Nickerson, R. M. White, K. N. Lee, R. Bachmann, T. H. Geballe, and G. W. Hull, Jr., *Phys. Rev. B* **3**, 2030 (1971).
- [33] R. S. Hayano, Y. J. Uemura, J. Imazato, N. Nishida, T. Yamazaki, and R. Kubo, *Phys. Rev. B* **20**, 850 (1979).
- [34] A. Schenck, *Muon Spin Rotation Spectroscopy: Principles and Applications in Solid State Physics* (Adam Hilger Ltd., Bristol, England, 1985).
- [35] See Supplemental Material at <http://link.aps.org/supplemental/10.1103/PhysRevLett.123.197203> for results from fits assuming the stretched-exponential parameter β changes with the applied longitudinal field.
- [36] X. Zhang, N. P. Butch, P. Syers, S. Ziemak, R. L. Greene, and J. Paglione, *Phys. Rev. X* **3**, 011011 (2013).
- [37] M. Shahrokhvand, S. Pezzini, M. R. van Delft, U. Zeitler, N. E. Hussey, and S. Wiedmann, *Phys. Rev. B* **96**, 205125 (2017).
- [38] B. Gorshunov, N. Sluchanko, A. Volkov, M. Dressel, G. Knebel, A. Loidl, and S. Kunii, *Phys. Rev. B* **59**, 1808 (1999).
- [39] A. B. Shick, L. Havela, A. I. Lichtenstein, and M. I. Katsnelson, *Sci. Rep.* **5**, 15429 (2015).
- [40] B. Skinner, *Phys. Rev. Mater.* **3**, 104601 (2019).
- [41] A. Yaouanc, P. Dalmass de Réotier, P. Bonville, G. Lebras, P. C. M. Gubbens, A. M. Mulders, and S. Kunii, *Europhys. Lett.* **47**, 247 (1999).
- [42] S. Kuroiwa, H. Takagiwa, M. Yamazawa, J. Akimitsu, A. Koda, R. Kadono, K. Ohishi, W. Higemoto, and I. Watanabe, *Sci. Technol. Adv. Mater.* **7**, 12 (2006).
- [43] J. Stankiewicz, P. F. S. Rosa, P. Schlottmann, and Z. Fisk, *Phys. Rev. B* **94**, 125141 (2016).
- [44] M. Orendáč, S. Gabáni, G. Pristáš, E. Gažo, P. Diko, P. Farkašovský, A. Levchenko, N. Shitsevalova, and K. Flachbart, *Phys. Rev. B* **96**, 115101 (2017).
- [45] B. Gorshunov, P. Haas, O. Ushakov, M. Dressel, and F. Iga, *Phys. Rev. B* **73**, 045207 (2006).
- [46] N. Shishiuchi, Y. Kato, O. M. Vyaselev, M. Takigawa, S. Hiura, F. Iga, and T. Takabatake, *J. Phys. Chem. Solids* **63**, 1231 (2002).